Journal of Applied Polymer Science

WILEY

Applied Polymer SCIENCE

RESEARCH ARTICLE OPEN ACCESS

Development and Characterization of Cellulose Films Incorporating Vitamin A and E-Loaded Liposomes

Nathalia Vieira Villar de Nunes[1] | Lincoln Audrew Cordeiro[1] | Camila Monteiro Cholant[1] | Ana Carolina Rodrigues Ribeiro[1] | João Pedro Almeida Lopes[1] | Everton Granemann Souza[2] | Chiara das Dores do Nascimento[1] | Alexandre Ferreira Galio[3] | Amanda Dantas de Oliveira[1] | Andre Ricardo Fajardo[1,4] | André Luiz Missio[1]

[1]Graduate Program in Materials Science and Engineering, Federal University of Pelotas (UFPel), Pelotas, RS, Brazil | [2]Graduate Program in Electronics and Computer Engineering, Catholic University of Pelotas (UCPel), Pelotas, RS, Brazil | [3]Graduate Program in Materials Science and Engineering, Federal University of Pampa (Unipampa), Bagé, RS, Brazil | [4]Graduate Program in Chemistry, Federal University of Pelotas (UFPel), Capão do Leão, RS, Brazil

Correspondence: André Luiz Missio (andreluizmissio@gmail.com)

Received: 19 November 2025 | **Revised:** 12 January 2026 | **Accepted:** 12 January 2026

Keywords: bioactive dressings | cellulose films | healing | sustainability | vitamin liposomes

ABSTRACT

This study introduces cellulose films enriched with vitamin A/E liposomes as sustainable, bioactive dressings for tattoo aftercare. Morphological analysis showed a smoother, more continuous microtexture than the neat cellulose films, while x-ray diffraction indicated reduced crystallinity upon liposome incorporation. Optically, the liposome–cellulose films combined strong ultraviolet shielding across 300–400 nm with visible transparency. Time-resolved contact-angle measurements placed them between neat cellulose and polyurethane, indicating controlled fluid uptake consistent with a moist, non-occlusive interface. Thermogravimetry revealed a higher peak degradation temperature with only a minimal change in onset. In uniaxial tension, the films reached a peak modulus of 16 GPa and maximum strength of 290 MPa at 50°C temperature, approaching high-performance nanocellulose benchmarks. Together, these results show that liposome–cellulose films integrate UV shielding, tunable wettability, and enhanced thermal-mechanical response, advancing a bio-based alternative to conventional dressings for newly tattooed skin.

1 | Introduction

The popularity of tattooing has increased markedly in recent years. Appropriate post-tattoo care, hygiene, moisturization, and photoprotection is essential to preserve appearance and prevent complications. Even with adequate hygiene, effects such as bleeding, crusting, swelling, photosensitivity, and skin infection may occur [1].

The market for tattoo aftercare products is evolving. Dexpanthenol-containing formulations are frequently recommended during the early healing phase due to their moisturizing and re-epithelialization support; however, they can also elicit allergic contact dermatitis [1, 2].

On the face of it, film dressings have gained traction, particularly transparent polyurethane (PU) sheets, because they are flexible, occlusive, and provide a barrier against external contaminants while maintaining visibility of the tattooed area. PU dressings are typically bioinert and petroleum-derived, offering little intrinsic bioactivity and raising sustainability questions. These limitations motivate the exploration of bio-based films that can combine moisture management with added functionality and improved biocompatibility [3].

All authors contributed equally to this article.

Cellulose is a promising alternative: an abundant, renewable, and tailorable biopolymer with potential to reduce plastic burden [4]. Depending on source and processing, it is cost-effective and widely used in pharmaceutical, paper, textile, biomedical, and composite applications [5].

A practical route to cellulose-based films is through hydrogels. Hydrogel dressings offer high water content at the wound interface, exudate management, oxygen permeability, and drug-release capability, and often provide superior moisture balance and patient comfort [6–10].

While cellulose hydrogels are attractive, neat cellulose does not inherently provide the full set of functions required by freshly tattooed skin as: sustained hydration, support for tissue regeneration, modulation of local inflammation, and sensory comfort [1, 11, 12]. Incorporating bioactive compounds is therefore desirable.

Prior studies have incorporated liposomes into polysaccharide films, including alginate/carboxymethyl-cellulose matrices embedding botanical actives and cellulose-derived films carrying liposomal antioxidants [13, 14]. Broader reviews likewise document liposomes in biopolymer platforms and their interfacial interactions [15, 16].

Nevertheless, the incorporation of vitamins A and E into water-based cellulose processing remains challenging because their high lipophilicity can drive macroscopic phase separation and localized vitamin-rich domains when added directly to aqueous hydrogels, undermining dispersion uniformity and reproducibility. Liposomal encapsulation provides a solvent-free route to introduce these actives into water-based cellulose matrices, favoring a more homogeneous distribution and potentially reducing premature losses by limiting exposure to oxygen and light [17–20].

However, to our knowledge there are no reports that integrate vitamin A/E liposomes specifically into cellulose films for tattoo aftercare and benchmark them head-to-head against commercial polyurethane (PU) dressings using a comprehensive structure–property workflow (SEM, XRD, FTIR, UV–Vis, wetting kinetics, TGA, and temperature-dependent tensile tests).

To address this gap, we propose enriching cellulose films with vitamin A/E liposomes. Although this study does not include biological testing such as cytocompatibility in skin-relevant cell models or irritation assessment for topical contact, it provides a rigorous materials-level foundation by reporting the fabrication route and the physicochemical and functional characterization of the resulting cellulose-liposome films.

2 | Experimental Materials and Methods

2.1 | Hydrogel Preparation

Cellulose hydrogels were produced following Missio et al. [21] with minor adaptations. An aqueous cellulose suspension at approximately 1.2 wt% was first premixed in a household blender (room temperature, ~2–3 min) to promote preliminary dispersion and to facilitate downstream refining. The cellulose content (1.2 wt%) was defined on a mass basis using the dry cellulose mass relative to the total suspension mass. The suspension was then processed in an ultrafine colloid mill (MKCA6–4, Masuko Sangyo Co. Ltd., Kawaguchi, Japan) operating at 1500 rpm between stone disks, with recirculation for 20 cycles, until a homogeneous hydrogel was obtained. No active temperature control was applied during milling. The process was carried out under laboratory ambient conditions. Homogeneity was assessed visually by the absence of visible agglomerates and by the formation of a continuous, uniform gel.

The vitamin A/E liposomal gel was supplied by a compounding pharmacy (Farmácia Curativa, Pelotas–RS, Brazil) and used as received. The liposomes were provided in a Carbopol-based gel containing 10 wt% vitamin A/E (in liposomal form). According to supplier specifications, the formulation presented an average hydrodynamic diameter of ~180 nm (dynamic light scattering, DLS), pH in the range 5–6, and encapsulation efficiencies higher than 89%.

For liposome-enriched hydrogels, the commercial vitamin A/E liposomal Carbopol gel was added during the premixing step at a fixed concentration of 3 wt% (relative to the total hydrogel), kept constant across all film formulations to isolate compositional effects. This corresponds to a nominal vitamin A/E loading of 0.3 wt% in the final hydrogel.

2.2 | Preparation of Bioactive Films

Bioactive films were cast to a target basis weight of 28 g m^{-2}. Considering the nominal vitamin A/E fraction in the hydrogel (0.3 wt%), this basis weight corresponds to a nominal vitamin A/E loading of 84 mg m^{-2} (8.4 μg cm^{-2}) in the cast films. Control films (CM) were prepared from cellulose-only hydrogels by casting onto silicone plates and drying at ambient temperature, following Ramos–Andrés et al. [22] with minor adaptations. Films containing vitamin A/E liposomes were prepared using the same casting protocol.

The overall workflow, from cellulose sourcing and hydrogel fabrication to incorporation of the commercial vitamin A/E liposomal gel and film casting, is summarized in the process schematic (Figure 1).

For benchmarking, we also analyzed a commercial polyurethane (PU) dressing-Tattoo Protection (Electric Ink, Uberaba, Brazil), alongside the neat cellulose (CM) and liposome–cellulose (CLM) films.

2.3 | Characterization of the Films

2.3.1 | Scanning Electron Microscopy (SEM)

Morphological characterization was carried out by scanning electron microscopy (SEM) (JEOL, JSM–6610LV) microscope equipped with an EDS microprobe. To ensure adequate electrical conductivity, samples were sputter–coated with gold prior to imaging. Images were acquired at 15 kV and magnifications of 500×, 1000×, and 3000×, allowing detailed evaluation of the surface morphology and microstructural features.

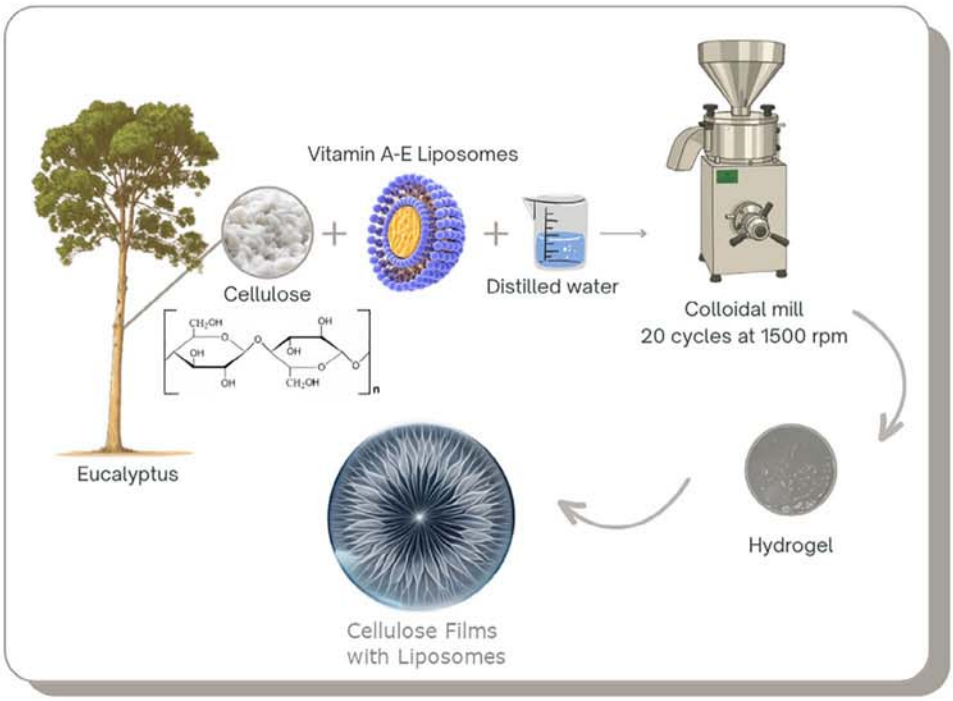

FIGURE 1 | Schematic of the process: Cellulose (from Eucalyptus fibers) is combined with vitamin A–E liposomes and refined in a colloid mill to form a hydrogel, which is then cast into a bioactive film. [Color figure can be viewed at wileyonlinelibrary.com]

2.3.2 | X– Ray Diffraction (XRD)

XRD patterns were recorded on a X-ray diffractometer (XRD 6000, Shimadzu, Kyoto, Japan) with Cu K α radiation, $\lambda = 1.5406$ Å. The instrument was operated at 30 kV and 30 mA. Scans were collected over $2\theta = 10^{\circ} - 60^{\circ}$ with a step speed of 1° min $^{-1}$. Data processing was performed using the XRD 6000 Software Package. The crystallinity index (CI) was calculated using Equation (1), as described by [23].

$$\mathrm{CI}(\%) = \frac{A_c}{A_c + A_a} \times 100 \quad (1)$$

where A_c and A_a are the areas of the crystalline and amorphous regions, respectively, obtained integrating the area under the XRD curves using OriginLab software [24].

2.3.3 | Fourier Transform Infrared Spectroscopy (FTIR)

Infrared spectra were acquired on a infrared spectrometer (Prestige–21, Shimadzu, Kyoto, Japan) equipped with an ATR accessory. Spectra were collected from 4000 to 600 cm^{-1} with a resolution of 4 cm^{-1} and 90 scans.

2.3.4 | Apparent Contact Angle

Surface wettability was evaluated by the sessile—drop method using an optical tensiometer Theta Lite (TL100, Biolin Scientific/Attension, Espoo, Finland) controlled by OneAttension software. Prior to testing, each film was mounted flat on the sample stage to minimize curvature and leveled according to the instrument procedure. For each sample, a 10 μL droplet of distilled water was gently deposited on a fresh area of the film surface, and five independent measurements were performed at spatially distinct locations to account for possible surface heterogeneity. The contact angle was monitored for 60 s with image acquisition at 20 frames s^{-1}, and the angle was determined using the software droplet– profile fitting routine. Reported values correspond to the mean of the five measurements, and the measurement variability did not exceed $\pm 2^{\circ}$ for any condition.

2.3.5 | Basis Weight (Grammage)

Basis weight (mass per unit area) was determined for the produced films. Squares of 1 cm × 1 cm were cut and weighed on an analytical balance; six specimens were measured per film type. Values were calculated according to TAPPI T 410 om-00 [25].

2.3.6 | Thickness and Density

The film thickness was measured with a Shahe digital micrometer. Apparent density was obtained from the ratio of basis weight to thickness, following TAPPI T220 om-01/om-02 [26]. The same 1 cm × 1 cm specimens used for basis weight were employed for thickness and density measurements.

2.3.7 | Water Uptake by Immersion

Water absorption was measured according to ASTM D570 [27] for plastics and polymeric films. Specimens were immersed in

water following a standardized protocol and the percentage uptake was computed by

$$\text{Absorption}(\%) = \frac{m_1 - m_0}{m_0} \times 100,$$

where m_0 is the initial dry mass (g) and m_1 is the mass after immersion (g). The primary immersion time was 2 min (according to TAPPI T491 [28] for papers and paperboards of intermediate absorbency). In a complementary test, samples were immersed for 1 h to assess stability and possible dissolution. After immersion, specimens were gently blotted to remove surface water and reweighed. Subsequently, films were analyzed by UV–Vis spectrophotometry over the same wavelength range described below.

2.3.8 | Ultraviolet–Visible (UV–Vis) Spectroscopy

Optical transmittance was measured with a single–beam UV–Vis spectrophotometer (UV-M51, Bel Engineering, Monza, Italy). Spectra were collected from 200 to 600 nm.

2.3.9 | Thermogravimetric Analysis (TGA)

Thermal stability and degradation behavior were evaluated by thermogravimetry using a DSC–60 unit (Shimadzu Corporation, Kyoto, Japan), operated in TGA mode. Samples were heated from 28°C to 600° C at 10° C. min $^{-1}$ under flowing nitrogen (50 mL. min $^{-1}$).

2.3.10 | Tensile Testing

Uniaxial tensile tests were performed on a Dynamic Mechanical Analyzer (Q800, TA Instruments, New Castle, DE, USA). Tests were conducted at 30°C, 40°C, 50°C, and 60° C with a heating rate of 4° C. min $^{-1}$ up to a maximum load of 18 N. Specimen dimensions were 30.00 mm (length) × 5.00 mm (width) with thickness between 0.15 and 0.20 mm. The following parameters were determined: maximum stress (σ_{max}), strain at break (ε), and elastic modulus (E). Prior to testing, specimens were conditioned at 23° C and 60% relative humidity for 24 h and kept sealed until measurement. All measurements were performed under a controlled room temperature of 23° C (± 2° C) and 60% (± 5%) relative humidity.

3 | Results and Discussion

3.1 | Macroscopic Appearance and Surface Morphology

Figure 2 shows the three types of films analyzed in the work: (a) the neat cellulose film (CM), (b) the cellulose film incorporating liposomes (CLM), and (c) a commercial polyurethane film (PU).

Visual inspection of Figure 2a shows that the CM exhibits a more irregular surface with small imperfections (bubbles), indicating heterogeneity of the polymeric network.

By contrast, the CLP (Figure 2b) presents a visibly smoother and more homogeneous surface, with no apparent bubbling or structural voids. Its more translucent and uniform appearance suggests a more even distribution of components, which can translate into improved properties as we will see in the next sections. For reference, Figure 2c shows a representative commercial polyurethane dressing used clinically for wound coverage.

Figure 3 presents a microstructural surface characterization by SEM, resolving the films' topography and morphology at the micrometer scale at 500×, 1000×, and 3000×.

The PU surface (Figure 3a) is uniform and compact, consistent with wound-dressing PU films described in the literature [29], suggesting an effective barrier against moisture loss and external contaminants. CM (Figure 3b) shows a rougher, less compact surface with exposed fibrils and micron-scale irregularities, features that can influence mechanical response and permeability [10]. This texture is consistent with the fibrous nature of cellulose.

SEM reveals that the CLM (Figure 3c) exhibits a smoother, more continuous topography than CM. This microstructural refinement is consistent with liposomes occupying interstitial voids within the cellulose network, enhancing cohesion and surface uniformity.

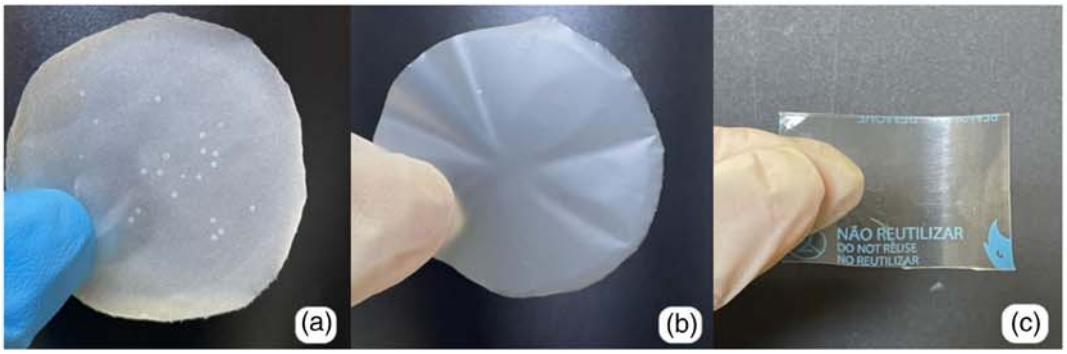

FIGURE 2 | Comparison of the three films studied: (a) neat cellulose film (CM), (b) the cellulose film incorporating liposomes (CLM), and (c) a commercial polyurethane film (PU). [Color figure can be viewed at wileyonlinelibrary.com]

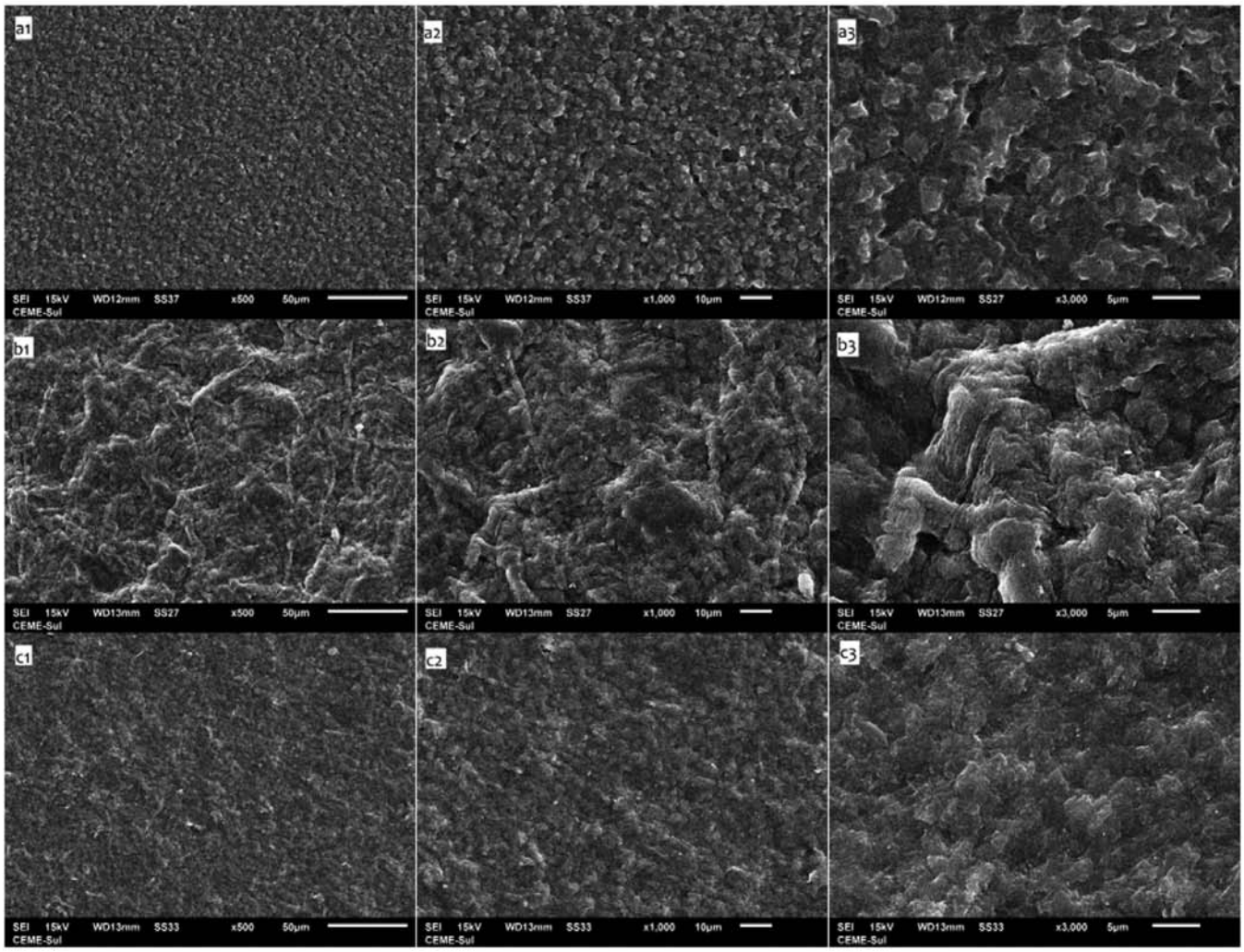

FIGURE 3 | Scanning electron micrographs of (a) PU, (b) CM, and (c) CLM at nominal magnifications of 1-500×, 2-1000×, and 3-3000×.

3.2 | Crystalline Structure Characterization by XRD

An X–ray diffraction (XRD) analysis was carried out to probe possible structural changes in the films. Measurements were performed at room temperature, and the diffractograms are shown in Figure 4.

The cellulose-based films (CM and CLM) display a broad maximum around $2\theta \approx 22^{\circ} - 23^{\circ}$ with few secondary reflections, characteristic of largely disordered (regenerated) cellulose. Liposome incorporation (CLM) further broadens and attenuates this maximum relative to CM, consistent with increased microstructural disorder and reduced crystallite size within the cellulose network. This characteristic is observed through the crystallinity index, evaluated by Equation (1), which decreases from 34.6% for the CM film to 23.6% for the CLM film, with this relative percentage reduction being approximately 32% after the incorporation of liposomes.

By contrast, the PU pattern shows a comparatively sharper feature near this angle, reflecting PU's own semicrystalline

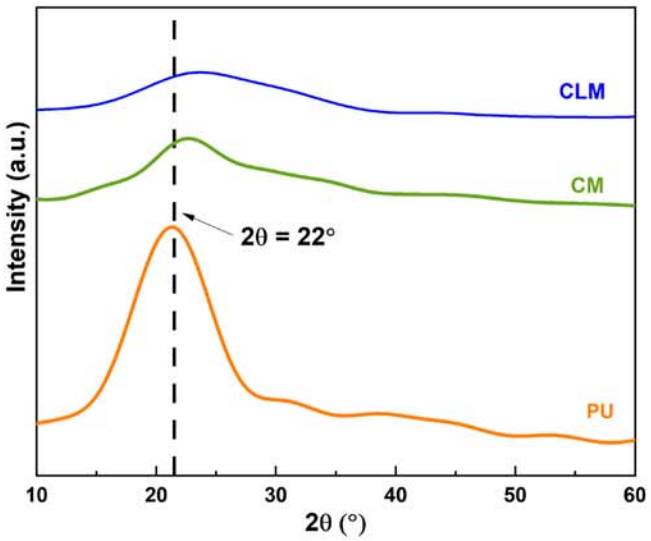

FIGURE 4 | XRD patterns of CM, CLM and, PU. Dashed lines indicate the peaks that occurs near $2\theta = 22^{\circ}$. [Color figure can be viewed at wileyonlinelibrary.com]

morphology (CI = 71.09%). Because PU is a different polymeric phase with distinct chemistry, scattering factors, and crystallographic motifs, its peak width and intensity will not be used to rank crystallinity against the cellulose films; they serve primarily as a phase fingerprint for PU.

3.3 | UV–Vis Transmittance

Figure 5a presents the UV–Vis transmittance spectra of CM, CLM, and PU in the 200–600 nm range. Its also included CLM after water immersion (CLM_{imm}, Figure 5b) to assess the effect of short-term hydration on optical clarity.

PU shows the highest visible transmittance (400–600 nm), CM the lowest, and CLM an intermediate, monotonic rise with wavelength. This ordering mirrors the SEM–derived surface uniformity (PU > CLM > CM): the compact, feature-poor PU surface minimizes diffuse scattering and thus transmits more light, whereas the rough, fibrillar CM surface enhances micro–scale scattering and depresses transmittance; CLM, whose liposomes smooth interstitial voids, lies in between. After immersion, CLM_{imm} exhibits a modest, reproducible drop in transmittance relative to CLM, consistent with slight swelling that increases refractive–index fluctuations and scattering; the spectral shape is otherwise preserved, indicating no optical damage.

In the UV (300–400 nm), chemistry dominates over microtexture: both cellulose–based films (CM and CLM) strongly attenuate UV relative to PU, reflecting intrinsic absorption by cellulose (and, for CLM, contributions from the liposomal/vitamin phase). CLM achieves slightly lower UV transmittance than CM, while CLM_{imm} is broadly comparable to CM. Practically, this strong UV attenuation (3–6 orders of magnitude greater than PU) makes CLM more suitable than PU for protecting newly tattooed skin; compared with CM, CLM offers marginally superior UV shielding while maintaining more controlled, non–occlusive moisture uptake.

3.4 | FTIR Analysis

Figure 6 shows the FTIR spectra of CM, CLM, and PU recorded at room temperature. FTIR provides an ensemble-averaged chemical fingerprint and, due to band overlap and non-unique assignments, it cannot unambiguously confirm specific interfacial bonding motifs, therefore, the discussion is presented as supportive evidence rather than definitive proof of a given interaction mechanism.

All samples display a broad envelope between 3700 and 3000 cm^{-1}, assigned to O—H stretching of cellulose and, in PU, overlapping N—H stretching from urethane/urea linkages. Aliphatic C—H stretching appears near 2920 cm^{-1} (and a weaker shoulder near 2850 cm^{-1}). The band at ~ 1650 cm^{-1}

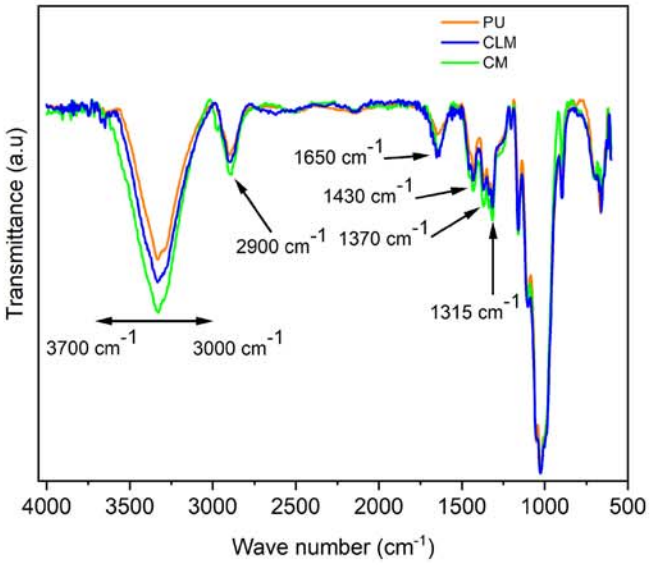

FIGURE 6 | FTIR spectra at room temperature of PU (orange), CLM (blue), and CM (green). Key bands are labeled (3700–3000, 2900, 1650, 1430, 1370, and 1315 cm^{-1}). [Color figure can be viewed at wileyonlinelibrary.com]

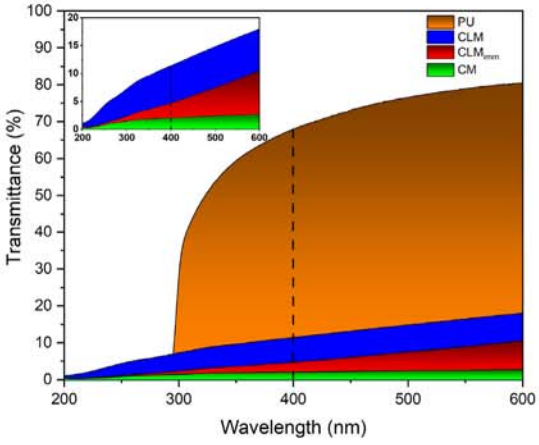

(a)

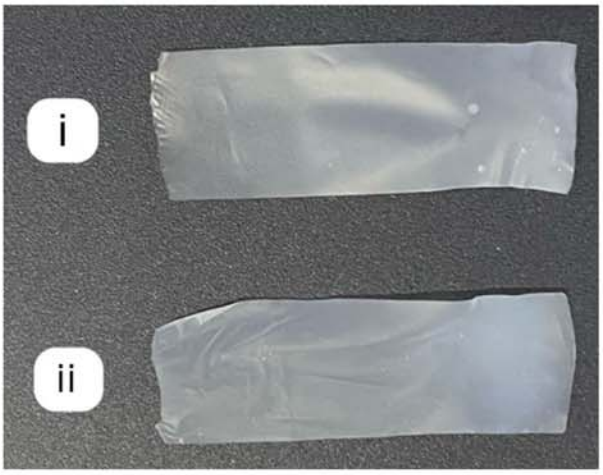

(b)

FIGURE 5 | (a) UV–Vis transmittance spectra (200–600 nm) of the three films: PU (orange), CLM (blue), CLMimm (CLM after water immersion, red) and CM (green). The dashed vertical line marks 400 nm (visible threshold). Inset: Magnified view of the low-transmittance region (0%–20%) for 200–600 nm. (b) (i) CLM and (ii) CLM after 1 h in water imersion. [Color figure can be viewed at wileyonlinelibrary.com]

corresponds to the H—O—H bending mode of absorbed water. Features around 1430, 1370, and 1315 cm^{-1} are consistent with CH_2 deformation/rocking and C—O—C/C—C skeletal vibrations in polysaccharides and related matrices [30–33].

In the O—H/N—H region, PU exhibits a lower overall intensity than the cellulose films, as expected for a material with fewer available hydroxyl donors. Conversely, CM shows the broadest and most intense O—H envelope, reflecting the high density of hydroxyl groups in cellulose. The CLM spectrum falls between PU and CM, consistent with partial interaction of the liposomal phase with the cellulose network and a concomitant redistribution of hydrogen bonds.

Pawlikowska et al. demonstrated that quercetin embedded in DPPC liposomes establishes hydrogen bonds between phenolic O—H groups and the phospholipid headgroup (phosphate-ester region) [34]. Because liposomes are typically phospholipid assemblies [15], an analogous scenario is plausible here: the observed band-shape changes in CLM (including subtle contributions in the mid-IR region) are *consistent with* increased polar interactions at the cellulose–liposome interface, potentially involving hydrogen bonding between cellulose hydroxyls and phospholipid headgroups and/or other noncovalent contacts (e.g., carbonyl/choline-associated interactions). However, due to spectral overlap, FTIR alone cannot isolate or prove a specific hydrogen-bonding configuration. Such interactions can broaden bands and induce small wavenumber shifts, which should be interpreted as qualitative, indirect indications of interfacial association rather than definitive evidence of a unique bonding mechanism.

In the aliphatic C—H region near 2920 cm^{-1}, the CLM spectrum often shows an intermediate intensity relative to CM and PU, which may reflect changes in local packing and segmental orientation due to hydrophobic (van der Waals) contacts between liposome alkyl chains and cellulose domains. Finally, the water bending band at ~ 1650 cm^{-1} is weakest for PU, in line with its comparatively higher hydrophobicity. Similar trends were reported for sodium—alginate/carboxymethylcellulose films incorporating green–tea liposomes, where the spectrum of the liposome–containing film lay between the liposome–free and liposome–rich cases [13].

Overall, the spectral changes are consistent with predominantly secondary interactions, hydrogen bonding, and other noncovalent contacts, rather than covalent bond formation between cellulose and the liposomal constituents.

3.5 | Wettability

The time evolution of the water contact angle for the three groups is shown in Figure 7. The red dashed line at 90° marks the conventional boundary between hydrophobic (> 90°) and hydrophilic (< 90°) wetting [35–37].

At $t = 0$ s, PU exhibited a water contact angle of ~ 91°, indicative of a predominantly hydrophobic surface. This value decreased slightly to ~ 85° at 60 s. The sustained near-spherical droplet shape suggests limited fluid-surface interaction and low liquid uptake, consistent with the typical behavior of polyurethane dressings.

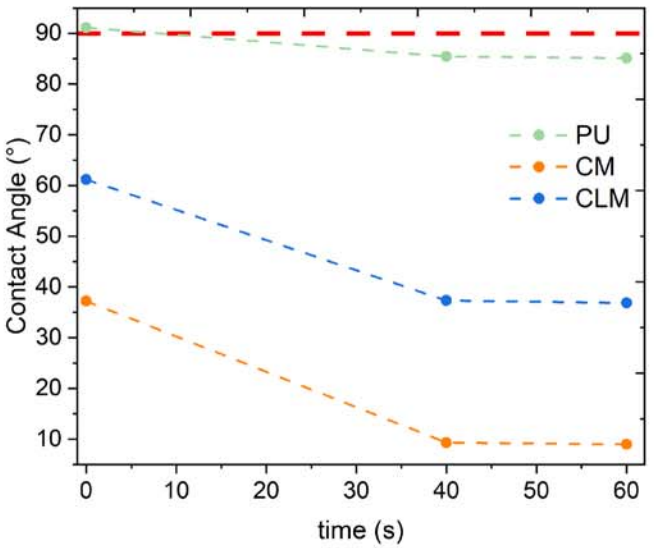

FIGURE 7 | Time-resolved water contact angle for PU, CM, and CLM over 60 s. The red dashed line at 90° marks the hydrophobic/hydrophilic threshold. Data points represent the mean of five measurements taken at different locations on each sample. The measurement variability did not exceed ± 2° for any condition. [Color figure can be viewed at wileyonlinelibrary.com]

In contrast, CM showed an initial contact angle below 37.5°, confirming its highly hydrophilic character, which decreased to ~ 9.4° by 40 s, with the droplet fully spreading across the surface. As discussed by Berglund et al. [38], the exponential decay of the contact angle arises from water migration into nanocellulose pores, facilitated by surface —OH groups that impart polarity and enable extensive hydrogen bonding [39], in agreement with the FTIR evidence.

The liposome-containing film, CLM, presented an intermediate response, with an initial angle of ~ 61.4° decreasing to ~ 37.1° at the experiment's end, indicative of a progressive, more controlled absorption process relative to CM. These results suggest that liposome incorporation can modulate fluid uptake, supporting a moist yet controlled microenvironment.

Commercial dressings frequently rely on synthetic polyurethane films to limit initial liquid ingress and provide an external barrier. Nevertheless, the literature emphasizes the need for materials that balance absorption and moisture retention to avoid excessive wound dehydration, particularly in hydroactive wound dressings [40, 41].

3.6 | Physicochemical Properties

CM and CLM films showed significant differences in their physical properties relative to each other and to PU, as illustrated in Figure 8.

The mean thickness (Figure 8a) and basis weight (Figure 8b) show that PU exhibited the greatest values, with a thickness of

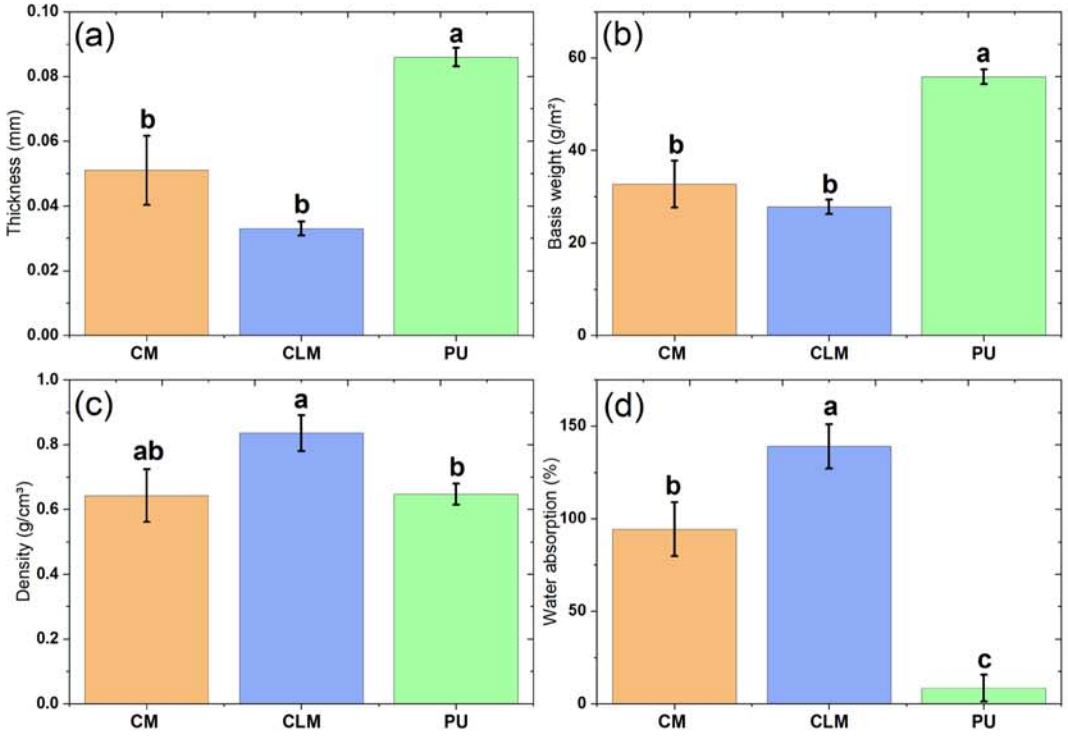

FIGURE 8 | Physicochemical properties of CM, CLM, and PU. Bars represent the mean and error bars indicate the standard deviation ($n = 6$). Within each panel, different superscript letters indicate significant differences between samples (two-tailed Welch's t-test with Holm correction, $\alpha = 0.05$). Grouping by panel: Thickness: {PU}^{a}, {CM, CLM}^{b}; Basis weight: {PU}^{a}, {CM, CLM}^{b}; Density: {CLM}^{a}, {CM}^{ab}, {PU}^{b}; Water absorption (2 min): {CLM}^{a}, {CM}^{b}, {PU}^{c}. [Color figure can be viewed at wileyonlinelibrary.com]

0.0868 ± 0.0025 mm and a basis weight of 57 ± 1.38 gm^{-2}. In both panels, PU differs significantly from the cellulose-based films (superscript a vs. b), whereas CM and CLM are not statistically different from each other (both b). An important point is that, although PU is the thickest and has the highest basis weight, it nevertheless exhibited the highest transmittance in the optical measurements (Section 3.3), indicating that material chemistry and microtexture outweigh thickness and grammage in governing light transmission.

CM presented lower values than PU, reaching 0.0518 ± 0.0102 mm in thickness and 33 ± 4.71 gm^{-2} in basis weight. This difference may be associated with supramolecular rearrangements of the cellulose network during regeneration and drying, which affect mass distribution and compaction [42].

CLM showed smaller mean values, with a thickness of 0.0335 ± 0.0021 mm and a basis weight of 28 ± 1.17 gm^{-2}. However, consistent with the statistical grouping (both b), these reductions relative to CM are not significant at $\alpha = 0.05$. The presence of liposomes appears to influence cellulose dispersion and modulate matrix reorganization (Section 3.1), promoting compaction and supporting a predominantly amorphous state, consistent with the XRD results (Section 3.2).

Density trends (Figure 8c) further support this interpretation: CLM shows a significantly higher density than PU (a vs. b), while CM is intermediate (ab) and therefore not statistically different from either material.

Finally, the mean water absorption results (Figure 8d) reveal marked differences among the three films. PU exhibited the lowest uptake, 9.0% ± 7.39%, as expected for a hydrophobic material. CM reached 95.0% ± 13.96%, whereas CLM attained 140.0% ± 11.8%. These differences are statistically significant and follow the ranking CLM > CM > PU (superscripts a, b, and c, respectively).

The higher uptake of CLM can be attributed to the amphiphilic nature of the liposomes [43], which can enhance water transport and retention within the film matrix by increasing free volume and enabling capillary-assisted penetration into internal voids. Importantly, the immersion test performed here captures early-stage uptake (2 min), where rapid capillary ingress and the onset of through-thickness swelling can be dominant, whereas the contact-angle experiment (Section 3.5) probes short-timescale sessile-drop wetting at the outer surface. Such a divergence is well documented for rough, absorbing substrates, where the apparent contact angle decreases over time due to droplet imbibition into surface-accessible pores, so the measured angle reflects both interfacial wetting and near-surface wicking rather than surface free energy alone [44, 45].

Consistent with the SEM observations (Section 3.1), CM exhibits a more open surface topography that favors faster imbibition and a steeper decay of the apparent contact angle, whereas CLM appears more cohesive at the outermost surface, leading to more controlled wetting kinetics. Under immersion, however, the liposomal phase may increase the film water-holding capacity by introducing hydrated amphiphilic domains and additional microvoid pathways, thereby enhancing through-thickness uptake and retention.

Importantly, although water a values may depend on film thickness and UV–Vis transmittance results (Section 3.3) may be influenced by both thickness and grammage, normalization only rescales the absolute magnitudes and does not change the relative ranking. This confirms that the main trends are not artifacts of thickness or basis-weight differences.

3.7 | Thermogravimetric Analysis (TGA)

Thermogravimetric analysis (TGA) was carried out to assess the thermal stability and degradation behavior of the films (Figure 9). Table 1 compiles the results, reporting the onset decomposition temperature (T_{onset}), the peak degradation temperature (T_{peak}), and the corresponding mass loss (weight (%)).

Figure 9a shows PU, which exhibits the highest thermal stability with $T_{onset} = 400.12^{\circ}$ C, $T_{peak} = 509.97^{\circ}$ C, and a mass loss of 95.81%, indicating near-complete degradation. CM (Figure 9b) displays $T_{onset} = 287.75^{\circ}$ C, $T_{peak} = 400.50^{\circ}$ C, and 55.04% mass loss, consistent with lower thermal stability relative to PU.

Upon liposome incorporation, CLM (Figure 9c) presents $T_{onset} = 282.62^{\circ}$ C, $T_{peak} = 416.40^{\circ}$ C, and 60.10% mass loss. Comparing the cellulose-based films, CLM attains a higher T_{peak} than CM while showing a slightly lower T_{onset} ($\approx 5^{\circ}$C). The implications of these thermal trends for mechanical performance are addressed in Section 3.8.

3.8 | Mechanical Performance at Elevated Temperature (Tensile Tests)

The uniaxial tensile response of the commercial polyurethane dressing (PU) and the cellulose-based films (CM and CLM) was evaluated at 30°C, 40°C, 50°C, and 60°C. The results are summarized in Tables 2 and 3 as mean ± standard deviation. Within each temperature and property, statistically significant differences among samples are indicated by different superscript letters.

TABLE 1 | Onset and peak temperatures for the main thermal decomposition stage, with associated mass loss (TGA/DTG).

Sample	T_{onset} (°C)	T_{peak} (°C)	Weight (%)
PU	400.12	509.97	95.81
CM	287.75	400.50	55.04
CLM	282.62	416.40	60.10

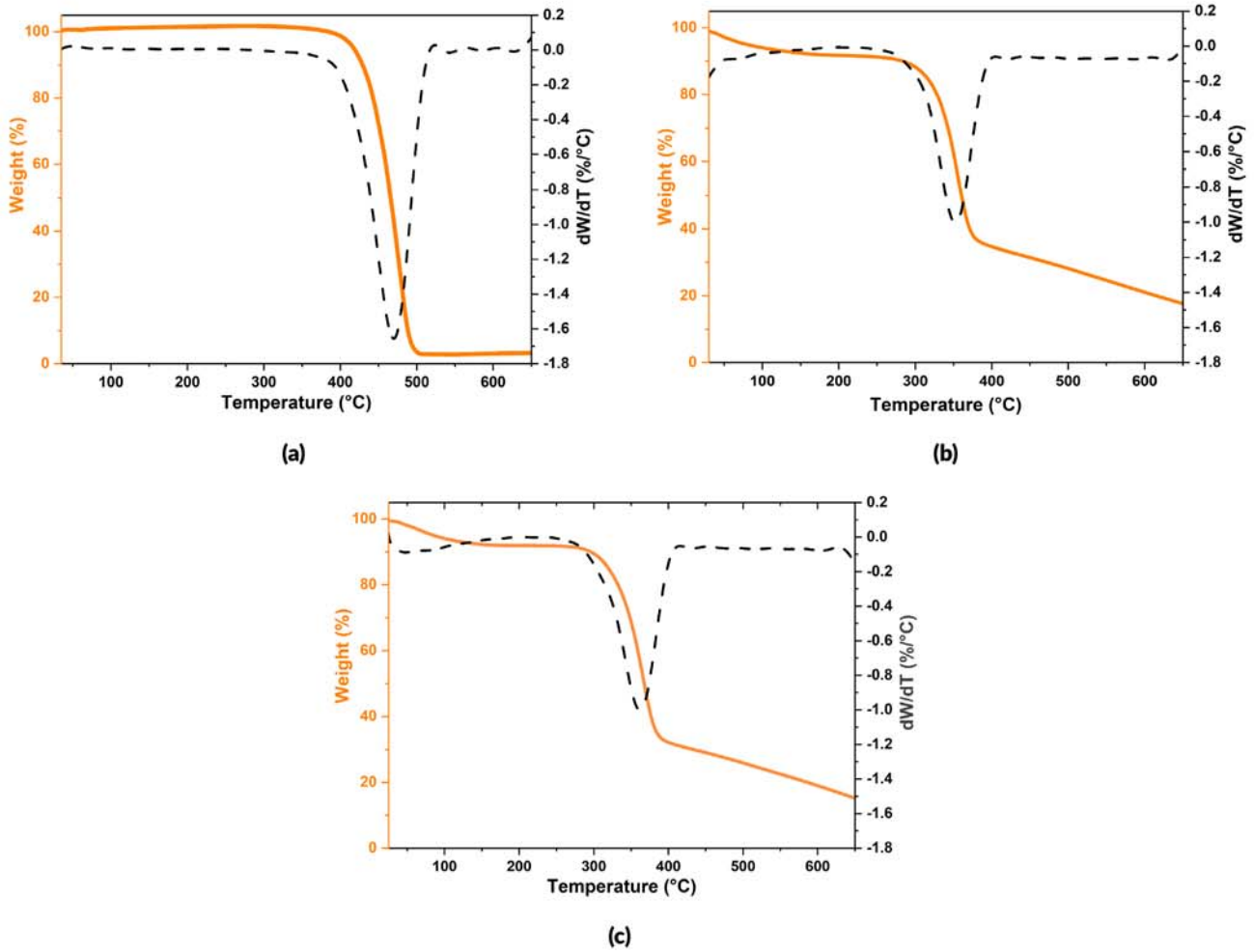

FIGURE 9 | TGA curves of: (a) PU, (b) CM and, (c) CLM. Orange: Mass loss (%). Black: Derivative (dW/dT, %/°C). [Color figure can be viewed at wileyonlinelibrary.com]

TABLE 2 | Mechanical properties of PU, CM, and CLM at 30°C and 40°C reported as mean ± standard deviation ($n = 3$): Ultimate tensile strength (σ_{max}), elongation at break (ε), and Young's modulus (E). Within each temperature and property, different superscript letters indicate significant differences between samples (two-tailed Welch's t-test with Holm correction, $\alpha = 0.05$). Grouping by column: At 30°C, σ_{max}: {PU, CLM}^{a}, {CM}^{b}; ε: {PU}^{a}, {CM, CLM}^{b}; E: {CLM}^{a}, {CM}^{b}, {PU}^{c}. At 40°C, σ_{max}: {CLM}^{a}, {PU, CM}^{b}; ε: {PU}^{a}, {CM}^{b}, {CLM}^{c}; E: {CLM}^{a}, {CM}^{b}, {PU}^{c}.

	30°C			40°C		
Sample	σ_{max} (MPa)	ε (%)	E (GPa)	σ_{max} (MPa)	ε (%)	E (GPa)
PU	59.83 ± 4.84^a	180.20 ± 9.30^a	0.21 ± 0.02^c	46.54 ± 3.77^b	295.70 ± 15.26^a	0.13 ± 0.01^c
CM	22.26 ± 1.80^b	6.03 ± 0.31^b	0.50 ± 0.04^b	48.27 ± 3.91^b	6.90 ± 0.36^b	0.80 ± 0.06^b
CLM	68.35 ± 5.53^a	6.46 ± 0.33^b	1.78 ± 0.13^a	90.20 ± 7.30^a	5.38 ± 0.28^c	2.62 ± 0.19^a

TABLE 3 | Mechanical properties of PU, CM, and CLM at 50°C and 60°C reported as mean ± standard deviation ($n = 3$): Ultimate tensile strength (σ_{max}), elongation at break (ε), and Young's modulus (E). Within each temperature and property, different superscript letters indicate significant differences between samples (two-tailed Welch's t-test with Holm correction, $\alpha = 0.05$). Grouping by column: At 50°C, σ_{max}: {CM, CLM}^{a}, {PU}^{b}; ε: {PU}^{a}, {CM}^{b}, {CLM}^{c}; E: {CLM}^{a}, {CM}^{b}, {PU}^{c}. At 60°C, σ_{max}: {CM}^{a}, {CLM}^{b}, {PU}^{c}; ε: {PU}^{a}, {CM}^{b}, {CLM}^{c}; E: {CLM}^{a}, {CM}^{b}, {PU}^{c}.

	50°C			60°C		
Sample	σ_{max} (MPa)	ε (%)	E (GPa)	σ_{max} (MPa)	ε (%)	E (GPa)
PU	34.06 ± 2.76^b	253.50 ± 13.08^a	0.07 ± 0.01^c	24.99 ± 2.02^c	447.60 ± 23.10^a	0.05 ± 0.01^c
CM	261.20 ± 21.13^a	7.87 ± 0.41^b	4.60 ± 0.34^b	278.40 ± 22.52^a	9.38 ± 0.48^b	4.37 ± 0.32^b
CLM	286.40 ± 23.17^a	3.31 ± 0.17^c	15.83 ± 1.17^a	133.70 ± 10.82^b	3.78 ± 0.20^c	6.30 ± 0.46^a

At 30°C, PU exhibited the highest ductility ($\varepsilon = 180.20\%$) and the lowest stiffness ($E = 0.21$ GPa), which is consistent with a soft and highly extensible elastomeric dressing. In contrast, both cellulose-derived films were brittle at this temperature ($\varepsilon \sim 6\%$). Despite their similarly low elongation, CLM was markedly stiffer than CM ($E = 1.78$ vs. 0.50 GPa, different letters), and its ultimate strength was significantly higher than CM. Notably, the ultimate strength of CLM and PU at 30°C did not differ statistically under the adopted test and analysis conditions (same letter in Table 2).

At 40°C, PU softened, as evidenced by reductions in both σ_{max} and E, while ε increased to 295.70%. In contrast, the cellulose-based films remained low-elongation materials ($\varepsilon < 7\%$). CLM showed the highest strength and stiffness at 40°C ($\sigma_{max} \approx 90$ MPa; $E \approx 2.62$ GPa), exceeding both PU and CM in σ_{max} and E, whereas PU and CM were not statistically different in σ_{max} at this temperature. These results indicate that liposome incorporation increased load-bearing capacity and rigidity relative to the cellulose-only film in the 30°C–40°C range.

At 50°C, Table 3, CM and CLM were statistically indistinguishable in σ_{max}, but CLM exhibited a significantly higher modulus, E, than CM (15.83 vs. 4.60 GPa) together with a significantly lower ε (3.31 vs. 7.87%), evidencing a ductility trade-off induced by liposome incorporation. This temperature-induced stiffening up to 50°C is consistent with the behavior of the cellulose-only film (CM), which also shows high strength and modulus at 50°C–60°C, supporting a thermal-conditioning effect of the regenerated-cellulose network. A plausible mechanistic interpretation is that heating promotes reduced plasticization (moisture loss) and supramolecular densification of the hydrogen-bonded cellulose structure, enhancing load-bearing and stress transfer within the fibrillar network.

At 60°C, all three materials differed statistically in σ_{max}, ε, and E, with CM presenting the highest σ_{max}, CLM retaining the highest modulus, and PU maintaining the highest elongation (Table 3). The pronounced decrease in CLM strength at 60°C (relative to its 50°C peak) suggests that additional temperature-dependent changes begin to dominate, plausibly including softening or structural rearrangement within the liposomal domains or at the liposome-cellulose interphase, which would reduce effective reinforcement and interfacial load transfer at higher temperature. This interpretation is compatible with a balance between temperature-enhanced network consolidation (up to 50°C) and subsequent thermal softening or interfacial rearrangements at higher temperature [46, 47].

For context, Rambabu et al. [48] reported nanocellulose films with tensile strength up to 273 MPa and modulus near 17 GPa. Under the 50°C condition, CLM reached a comparable modulus (15.83 GPa), indicating that the cellulose-based network can approach nanocellulose-like rigidity even in the presence of liposomal domains, albeit with very limited strain-to-failure.

These results reinforce two distinct mechanical profiles: PU behaves as a highly extensible, temperature-softening elastomer, whereas CM/CLM remain low-elongation, high-stiffness films. Within the cellulose-based group, CLM tends to increase stiffness relative to CM at 30°C–50°C, but at 60°C the strength ranking reverses (CM > CLM), confirming that liposome incorporation modifies not only the absolute mechanical level but also its temperature sensitivity.

4 | Conclusions

Incorporating vitamin A/E liposomes into regenerated–cellulose films produced a smoother, more continuous microtexture (SEM) and a broader, less intense diffraction maximum relative to neat cellulose (XRD), consistent with increased structural disorder without introducing PU-like crystalline features.

Optically, the liposome–cellulose films (CLM) maintained visible transparency between that of PU and neat cellulose while delivering strong ultraviolet attenuation (300–400 nm), slightly surpassing the cellulose control and far outperforming PU; after short water immersion, the spectral shape was preserved, indicating no optical damage.

Contact-angle kinetics positioned CLM between hydrophobic PU and highly hydrophilic cellulose, evidencing controlled fluid uptake suitable for a moist, non-occlusive interface.

Thermogravimetry showed an increased peak degradation temperature for CLM (416.4°C) versus cellulose (400.5°C) with only a modest decrease in onset ($\sim 5^{\circ}$C), indicating strengthened thermal response without loss of integrity. Under uniaxial tension, CLM reached its best performance at 50°C (strength ≈286.4 MPa; modulus ≈15.83 GPa), surpassing neat cellulose and approaching benchmarks for high-performance nanocellulose films.

Taken together, CLM combines UV shielding, tunable wettability, and enhanced thermo-mechanical performance in a renewable platform, advancing a credible bio-based alternative to polyurethane dressings for newly tattooed skin.

As limitations of this study, further validation is required to support skin-contact applicability beyond materials performance, including: (i) quantitative vitamin A/E release kinetics under relevant aqueous/sweat-mimicking conditions; (ii) in vitro cytocompatibility using appropriate skin-relevant cell models; and (iii) irritation/sensitization assessment appropriate for topical contact. In addition, functional performance under realistic use conditions should be verified (adhesion and wear under sweat/UV/rubbing), together with antimicrobial screening and, where applicable, in vivo evaluation to confirm safety and efficacy.

Author Contributions

Nathalia Vieira Villar de Nunes: conceptualization (equal), data curation (equal), formal analysis (equal), investigation (equal), methodology (equal), validation (equal), writing – original draft (equal), writing – review and editing (equal). **Lincoln Audrew Cordeiro:** data curation (equal), formal analysis (equal), software (equal), validation (equal). **Camila Monteiro Cholant:** formal analysis (equal), investigation (equal), software (equal), validation (equal). **Ana Carolina Rodrigues Ribeiro:** formal analysis (equal), software (equal), visualization (equal). **João Pedro Almeida Lopes:** formal analysis (equal), investigation (equal), validation (equal). **Everton Granemann Souza:** formal analysis (equal), investigation (equal), software (equal), validation (equal), writing – original draft (lead), writing – review and editing (equal). **Chiara das Dores do Nascimento:** conceptualization (equal), data curation (equal), methodology (equal), supervision (equal), writing – original draft (equal), writing – review and editing (equal). **Alexandre Ferreira Galio:** formal analysis (equal), investigation (equal), supervision (equal), writing – review and editing (equal). **Amanda Dantas de Oliveira:** formal analysis (equal), investigation (equal), methodology (equal), resources (equal), writing – review and editing (equal). **Andre Ricardo Fajardo:** conceptualization (equal), methodology (equal), resources (equal), supervision (equal), writing – review and editing (equal). **André Luiz Missio:** conceptualization (equal), formal analysis (equal), funding acquisition (lead), investigation (equal), methodology (equal), resources (lead), supervision (lead).

Acknowledgments

The authors gratefully acknowledge the Coordenação de Aperfeiçoamento de Pessoal de Nível Superior (CAPES), Brazil, Finance Code 001, for the financial support.

Funding

This work was supported by Coordenação de Aperfeicoamento de Pessoal de Nível Superior (grant no. Finance Code 001).

Conflicts of Interest

The authors declare no conflicts of interest.

Data Availability Statement

The datasets generated during and/or analyzed during the current study are available from the corresponding author on reasonable request.

References

1. D. A. Schmid, M. P. Domingues, A. Nanu, N. Kluger, R. de Salvo, and S. Trapp, "Exploratory Evaluation of Tolerability, Performance, and Cosmetic Acceptance of Dexpanthenol-Containing Dermo-Cosmetic Wash and Sun-Care Products for Tattoo Aftercare," *Health Science Reports* 5, no. 4 (2022): e635, https://doi.org/10.1002/hsr2.635.

2. S. A. Temiz and E. Özlü, "Medical Complications of Tattoos," *Journal of the Turkish Academy of Dermatology* 15, no. 1 (2021): 1–7, https://doi.org/10.4274/jtad.galenos.2021.02486.

3. Y. Liu, S. Gao, J. Liu, and Q. Zhang, "Biomimetic Slippery Liquid-Infused Porous Surfaces Fabricated by Porous Fluorinated Polyurethane Films for Anti-Icing Property," *Progress in Organic Coatings* 179 (2023): 107524, https://doi.org/10.1016/j.porgcoat.2023.107524.

4. L. Jin, J. Xu, Q. Yang, et al., "Fabrication of Cellulose/Rectorite Composite Films for Sustainable Packaging," *International Journal of Biological Macromolecules* 224 (2023): 1471–1477, https://doi.org/10.1016/j.ijbiomac.2022.10.234.

5. Z. Han, H. Zhu, and J. Cheng, "Structure Modification and Property Improvement of Plant Cellulose Based on Emerging and Sustainable Nonthermal Processing Technologies," *Food Research International* 156 (2022): 111300, https://doi.org/10.1016/j.foodres.2022.111300.

6. X. Huang, Y. Ji, L. Guo, et al., "Incorporating Tannin Onto Regenerated Cellulose Film Towards Sustainable Active Packaging," *Industrial Crops and Products* 180 (2022): 114710, https://doi.org/10.1016/j.indcrop.2022.114710.

7. S. Huang, H. J. Chen, Y. P. Deng, X. Hua You, Q. Hui Fang, and M. Lin, "Preparation of Novel Stable Microbicidal Hydrogel Films as Potential Wound Dressing," *Polymer Degradation and Stability* 181 (2020): 109349, https://doi.org/10.1016/j.polymdegradstab.2020.109349.

8. L. C. Wong, J. H. Poh, W. T. Tan, et al., "Cellulose Hydrogel Development From Unbleached Oil Palm Biomass Pulps for Dermal Drug Delivery," *International Journal of Biological Macromolecules* 224 (2023): 483–495, https://doi.org/10.1016/j.ijbiomac.2022.10.138.

9. D. Kotlarek, K. Liu, N. G. Quilis, et al., "Thin-Film Polyisocyanide-Based Hydrogels for Affinity Biosensors," *Journal of Physical Chemistry C* 125 (2021): 12960–12967, https://doi.org/10.1021/acs.jpcc.1c02489.

10. A. Subhedar, S. Bhadauria, S. Ahankari, and H. Kargarzadeh, "Nanocellulose in Biomedical and Biosensing Applications: A Review," *International Journal of Biological Macromolecules* 166 (2021): 587–600, https://doi.org/10.1016/j.ijbiomac.2020.10.217.

11. A. Fauger, S. Sonck, N. Kluger, M. Chavagnac-Bonneville, and M. Sayag, "Tattoo Aftercare Management With a Dermo-Cosmetic Product: Improvement in Discomfort Sensation and Skin Repair Quality," *Journal of Cosmetic Dermatology* 21, no. 3 (2022): 1051–1056, https://doi.org/10.1111/jocd.14157.

12. T. Lin, L. Zhong, and J. Santiago, "Anti-Inflammatory and Skin Barrier Repair Effects of Topical Application of Some Plant Oils," *International Journal of Molecular Sciences* 19 (2017): 70, https://doi.org/10.3390/ijms19010070.

13. X. Feng, Y. Li, Z. Cui, and R. Tang, "Sodium Alginate/Carboxymethyl Cellulose Films Embedded With Liposomes Encapsulated Green Tea Extract: Characterization, Controlled Release, Application," *RSC Advances* 14 (2024): 245–254, https://doi.org/10.1039/D3RA05196J.

14. C. Vidal, J. Lopez-Polo, and F. A. Osorio, "Physical Properties of Cellulose Derivative-Based Edible Films Elaborated With Liposomes Encapsulating Grape Seed Tannins," *Antioxidants* 13, no. 8 (2024): 989, https://doi.org/10.3390/antiox13080989.

15. B. S. Esposto, P. Jauregi, D. R. Tapia-Blácido, and M. Martelli-Tosi, "Liposomes vs. Chitosomes: Encapsulating Food Bioactives," *Trends in Food Science & Technology* 108 (2021): 40–48, https://doi.org/10.1016/j.tifs.2020.12.003.

16. H. Nsairat, D. Khater, U. Sayed, F. Odeh, A. Al Bawab, and W. Alshaer, "Liposomes: Structure, Composition, Types, and Clinical Applications," *Heliyon* 8, no. 5 (2022): e09394, https://doi.org/10.1016/j.heliyon.2022.e09394.

17. J. Zhong, N. Zhao, Q. Song, Z. Du, and P. Shu, "Topical Retinoids: Novel Derivatives, Nano Lipid-Based Carriers, and Combinations to Improve Chemical Instability and Skin Irritation," *Journal of Cosmetic Dermatology* 23, no. 10 (2024): 3102–3115, https://doi.org/10.1111/jocd.16415.

18. V. Saez, I. D. L. Souza, and C. R. E. Mansur, "Lipid Nanoparticles (SLN & NLC) for Delivery of Vitamin E: A Comprehensive Review," *International Journal of Cosmetic Science* 40, no. 2 (2018): 103–116, https://doi.org/10.1111/ics.12452.

19. M. A. Rahim, H. A. Zahran, H. M. Jaffar, et al., "Liposomal Encapsulation in Food Systems: A Review of Formulation, Processing, and Applications," *Food Science & Nutrition* 13, no. 8 (2025): e70587, https://doi.org/10.1002/fsn3.70587.

20. H. Liu, J. Zhang, Y. Xiong, et al., "Improving Norbixin Dispersibility and Stability by Liposomal Encapsulation Using the pH-Driven Method," *Journal of the Science of Food and Agriculture* 102, no. 5 (2022): 2070–2079, https://doi.org/10.1002/jsfa.11546.

21. A. L. Missio, B. D. Mattos, D. de F Ferreira, et al., "Nanocellulose-Tannin Films: From Trees to Sustainable Active Packaging," *Journal of Cleaner Production* 184 (2018): 143–151, https://doi.org/10.1016/j.jclepro.2018.02.205.

22. M. Ramos-Andrés, L. Hu, H. Grénman, C. Xu, and J. García-Serna, "Upcycling of Carrot Waste Into Pectin-Arabinogalactan and Lignin-Cellulose Films via Hydrothermal Treatment, Ultrafiltration/Diafiltration, and Casting," *Journal of Environmental Chemical Engineering* 12, no. 3 (2024): 112645, https://doi.org/10.1016/j.jece.2024.112645.

23. M. W. Bosenbecker, E. V. Silva, P. O. Schmitt, et al., "Improved Thermal and Structural Performance of LDPE Reinforced With Bamboo Cellulose Nanocrystals via PE-g-MA Compatibilization," *Journal of Applied Polymer Science* 142 (2025): e58181, https://doi.org/10.1002/app.58181.

24. *OriginPro 2023 (Student Version): User Guide* (OriginLab Corporation, 2023), https://www.originlab.com/.

25. TAPPI, *T 410: Grammage of Paper and Paperboard (Weight Per Unit Area)* (TAPPI, 2000) Official Method. TAPPI Test Method T 410 om-00.

26. TAPPI, *T 220: Physical Testing of Pulp Handsheets* (TAPPI, 2001) Official Method. TAPPI Test Method T 220 om-01.

27. ASTM International, *ASTM D570-98: Standard Test Method for Water Absorption of Plastics* (TAPPI, 1998) Committee D20 on Plastics. ASTM Standard D570-98.

28. TAPPI, *T 491: Water Immersion Test of Paperboard* (TAPPI, 2023) Official Method. TAPPI/ANSI Test Method T 491 om-23.

29. A. Alberts, D. I. Tudorache, A. G. Niculescu, and A. M. Grumezescu, "Advancements in Wound Dressing Materials: Highlighting Recent Progress in Hydrogels, Foams, and Antimicrobial Dressings," *Gels* 11 (2025): 11, https://doi.org/10.3390/gels11020123.

30. J. Wang, Y. Song, F. Cui, et al., "Preparation and Characterization of Nanocellulose Fiber (CNF) by Biological Enzymatic Method," *Journal of Thermoplastic Composite Materials* 37, no. 3 (2023): 1223–1241, https://doi.org/10.1177/08927057231180479.

31. R. C. M. Dias, A. M. Góes, R. Serakides, E. Ayres, and R. L. Oréfice, "Porous Biodegradable Polyurethane Nanocomposites: Preparation, Characterization, and Biocompatibility Tests," *Materials Research* 13, no. 2 (2010): 211–218, https://doi.org/10.1590/S1516-14392010000200015.

32. R. A. Ilyas, S. M. Sapuan, and M. R. Ishak, "Isolation and Characterization of Nanocrystalline Cellulose From Sugar Palm Fibres (*Arenga Pinnata*)," *Carbohydrate Polymers* 181 (2018): 1038–1051, https://doi.org/10.1016/j.carbpol.2017.11.045.

33. R. R. Ferreira, A. G. Souza, L. L. Nunes, N. Shahi, V. K. Rangari, and R. D. dos Santos, "Use of Ball Mill to Prepare Nanocellulose From Eucalyptus Biomass: Challenges and Process Optimization by Combined Method. Materials Today," *Communications* 22 (2020): 22, https://doi.org/10.1016/j.mtcomm.2019.100755.

34. B. Pawlikowska-Pawlega, H. Dziubińska, E. Król, et al., "Characteristics of Quercetin Interactions With Liposomal and Vacuolar Membranes," *Biochimica et Biophysica Acta (BBA) - Biomembranes* 1838, no. 1 (2014): 254–265, https://doi.org/10.1016/j.bbamem.2013.08.014.

35. M. F. Ismail, M. A. Islam, B. Khorshidi, A. Tehrani-Bagha, and M. Sadrzadeh, "Surface Characterization of Thin-Film Composite Membranes Using Contact Angle Technique: Review of Quantification Strategies and Applications," *Advances in Colloid and Interface Science* 299 (2022): 299, https://doi.org/10.1016/j.cis.2021.102524.

36. H. N. Giang, T. X. Nguyen, T. V. Huynh, et al., "Fabrication of Superhydrophobic Surface Using One-Step Chemical Treatment," *Surfaces and Interfaces* 21 (2020): 100673, https://doi.org/10.1016/j.surfin.2020.100673.

37. C. D. Nascimento, E. G. Souza, C. Aguzzoli, and R. L. Cruz, "Effects of Oxygen on the Resistivity in au Thin Films With Ti-Al Adhesion Layer," *Journal of Vacuum Science & Technology B* 37, no. 5 (2019): 052202, https://doi.org/10.1116/1.5119099.

38. L. Berglund, P. Squinca, Y. Baş, et al., "Self-Assembly of Nanocellulose Hydrogels Mimicking Bacterial Cellulose for Wound Dressing Applications," *Biomacromolecules* 24 (2023): 2264–2277, https://doi.org/10.1021/acs.biomac.3c00152.

39. M. R. Fischer, M. C. F. Garcia, A. L. Nogueira, L. M. Porto, A. L. S. Schneider, and A. P. T. Pezzin, "Biossíntese e Caracterização de Nanocelulose Bacteriana Para Engenharia de Tecidos," *Revista Matéria* 22 (2017): 22, https://doi.org/10.1590/S1517-707620170005.0270.

40. M. Morales-González, L. E. Díaz, C. Dominguez-Paz, and M. F. Valero, "Insights Into the Design of Polyurethane Dressings Suitable for the Stages of Skin Wound-Healing: A Systematic Review," *Polymers* 14 (2022): 14, https://doi.org/10.3390/polym14152990.

41. W. Liang, N. Ni, Y. Huang, and C. Lin, "An Advanced Review: Polyurethane-Related Dressings for Skin Wound Repair," *Polymers* 15 (2023): 15, https://doi.org/10.3390/polym15214301.

42. H. M. A. Ehmann, O. Werzer, S. Pachmajer, et al., "Surface-Sensitive Approach to Interpreting Supramolecular Rearrangements in Cellulose by Synchrotron Grazing Incidence Small-Angle X-Ray Scattering," *ACS Macro Letters* 4 (2015): 713–716, https://doi.org/10.1021/acsmacrolett.5b00306.

43. S. Hossen, M. K. Hossain, M. K. Basher, M. N. H. Mia, M. T. Rahman, and M. J. Uddin, "Smart Nanocarrier-Based Drug Delivery Systems for Cancer Therapy and Toxicity Studies: A Review," *Journal of Advanced Research* 15 (2019): 1–18, https://doi.org/10.1016/j.jare.2018.06.005.

44. S. Krainer and U. Hirn, "Contact Angle Measurement on Porous Substrates: Effect of Liquid Absorption and Drop Size," *Colloids and Surfaces A: Physicochemical and Engineering Aspects* 619 (2021): 126503, https://doi.org/10.1016/j.colsurfa.2021.126503.

45. M. A. Hubbe, D. J. Gardner, and W. Shen, "Contact Angles and Wettability of Cellulosic Surfaces: A Review of Proposed Mechanisms and Test Strategies," *BioResources* 10, no. 4 (2015): 8657–8749, https://doi.org/10.15376/biores.10.4.Hubbe_Gardner_Shen.

46. O. Mertins, P. H. Schneider, A. R. Pohlmann, and N. P. da Silveira, "Interaction Between Phospholipids Bilayer and Chitosan in Liposomes Investigated by ^{31}P NMR Spectroscopy," *Colloids and Surfaces B: Biointerfaces* 75, no. 1 (2010): 294–299, https://doi.org/10.1016/j.colsurfb.2009.08.048.

47. C. Meireles Batista, M. Barros, C. de Carvalho, N. Stela, S. Magalhães, and N. S. S. Magalhães, "Lipossomas e Suas Aplicações Terapêuticas: Estado da Arte," *Revista Brasileira de Ciências Farmacêuticas* 43 (2007): 43–179, https://doi.org/10.1590/S1516-93322007000200003.

48. N. Rambabu, S. Panthapulakkal, M. Sain, and A. K. Dalai, "Production of Nanocellulose Fibers From Pinecone Biomass: Evaluation and Optimization of Chemical and Mechanical Treatment Conditions on Mechanical Properties of Nanocellulose Films," *Industrial Crops and Products* 83 (2016): 746–754, https://doi.org/10.1016/j.indcrop.2015.11.083.